Supplementary information for

Oxygen Vacancies Enriched Sub-Nanometer CoPd Hybrid Clusters Promotes the CO production Yield of Cobalt-Oxide Supported Pd Nanoparticles

Che Yan,[1‡] Dinesh Bhalothia,[1‡] Shou-Shiun Yang,[1] Amisha Beniwal,[1] You-Xun Chang,[1] Pin-Chieh Wang,[1] Yu-Chia Cheng,[1] Chi-Liang Chen,[2] Shun-Chi Wu,[1] and Tsan-Yao Chen [1, 3*]

Affiliations:

[1] Department of Engineering and System Science, National Tsing Hua University, Hsinchu 30013, Taiwan

[2] National Synchrotron Radiation Research Center, Hsinchu 30076, Taiwan

[3] Hierarchical Green-Energy Materials (Hi-GEM) Research Centre, National Cheng Kung University, Tainan 70101, Taiwan

‡ denotes equal contribution of authors.

Corresponding Author:

Tsan-Yao Chen

Email: chencaeser@gmail.com

Tel: +886-3-5715131 # 34271

FAX: +885-3-5720724

1. Physical Characterizations of Experimental Nanocatalysts.

The physical properties of CP-CoO$_x{}^V$Pd as well as reference samples were investigated by the cross-referencing results of electron microscopy and X-ray spectroscopic techniques. The high-resolution transmission electron microscope (HRTEM) images were obtained at the National Tsing Hua University, Taiwan for revealing the crystal structure and surface morphology of as-prepared samples. The XRD spectra were measured at the beamline of BL-01C2 of the National Synchrotron Radiation Research Center (NSRRC), Taiwan with an incident X-ray of wavelength 0.6888 Å (18.0 KeV). The X-ray absorption spectroscopy (XAS) of experimental samples was executed at beamlines BL-17C and 01C1 of NSRRC, Taiwan and normalized by using ATHENA software. For the extended X-ray absorption fine structure (EXAFS) analysis, the backgrounds of the pre-edge and the post-edge were subtracted and normalized to the edge jump step from the XAS spectra. The normalized spectra were transformed from energy to k-space and further weighted by k^3 to distinguish the contributions of backscattering interferences from different coordination shells. Normally, the backscattered amplitude and phase shift functions for specific atom pairs were theoretically estimated by utilizing the FEFF8.0 code. The X-ray photoelectron spectroscopy (XPS) (Thermo VG Scientific Sigma Probe, operated at a voltage of 20 kV and a current of 30 mA) with a monochromatic X-ray source (Al Kα) was employed to investigate the oxidation states and surface compositions of the experimental samples. The surface compositions of the samples were estimated by calculating the integral of each peak. Shirley-type background was used to subtract the original peak, and then a combination of Lorentzian and Gaussian lines was applied to fit the experimental curve. Accurate binding energies were determined by reference to the C 1s peak at 284.6 eV.

2. Electrochemical Analysis

The electrochemical measurements were carried out at room temperature using a potentiostat (CH Instruments Model 600B, CHI 600B) equipped with a three-electrode system. The catalyst slurry was prepared by ultrasonic dispersion of 5 mg catalyst powder in 1.0 ml of isopropanol (IPA) and 50 μl of Nafion-117 (99%, Sigma-Aldrich Co.). For conducting the electrochemical measurements, 10.0 μl of catalyst slurry was dropped and air-dried on a glassy carbon rotating disk electrode (RDE) (0.196 cm^2 area) as a working electrode. Hg/HgCl$_2$ (the voltage was calibrated by 0.242 V, in alignment with that of RHE) electrode saturated in KCl aqueous solution was used as the reference electrode. Whereas, a Pt wire was employed as the counter electrode. The cyclic voltammetry (CV) curves were obtained at the voltage scan rate of 0.02 V s^{-1} and the potential range of 0.1 V to 1.3 V (V vs RHE.) in an N$_2$ saturated 0.1 M KOH electrolyte (pH 13). Besides, Ag/AgCl electrode were used as the reference electrode for CO-stripping analysis. The adsorption of CO on the surface of the catalyst was performed by purging CO into 0.5 M H$_2$SO$_4$ at 0.05 V (vs NHE) for 20 min. Then the CO stripping voltammetry was measured between -0.10 and 1.20 V (vs NHE) in N$_2$ saturated 0.5 M H$_2$SO$_4$ solution at a scan rate of 50 mVs^{-1}.

3. Comparison of selected catalysts in RWGS.

Table S1. Benchmark of catalysts for RWGS application

Composition	Feed gas	Temp. (°C)	S$_{CO}$ (%)	Reference
CP-CoO$_x{}^V$Pd	CO$_2$:H$_2$ = 1:3 [a]	250	98.9	This work
12CuAl-GD/Al$_2$O$_3$	CO$_2$:H$_2$ = 1:4 [b]	400	100	1
FeCuCs/Al$_2$O$_3$	CO$_2$:H$_2$ = 1:4 [c]	400	100	2
Cu-Ce/CDC	CO$_2$:H$_2$ = 1:4 [c]	500	100	3
1.0 wt% Ni/CeO$_2$	CO$_2$:H$_2$ = 1:4 [b]	300	100	4
Ni	CO$_2$:H$_2$ = 1:4	550	99.5	5
0.25Fe0.75Cu	CO$_2$:H$_2$ = 1:4	450	100	6

Mo(0.8)Co(0.2)/FAU	$CO_2:H_2 = 1:1$ [c]	500	99	7
NiCu	$CO_2:H_2 = 1:4$ [c]	700	93	8
1%NiCo/SiO$_2$	$CO_2:H_2 = 1:4$	700	90	9
MoO$_3$/Ti$_3$AlC$_2$	$CO_2:H_2 = 1:4$	559	~90	10
Co(10)/ZrO$_2$	$CO_2:H_2 = 1:4$ [d]	340	97	11

[a]: without carrier gas
[b]: carrier gas: Ar
[c]: carrier gas: N$_2$
[d]: 3 MPa pressure

4. Low magnification TEM image of Pd/AC and CP-CoO$_x$^{V}Pd NCs.
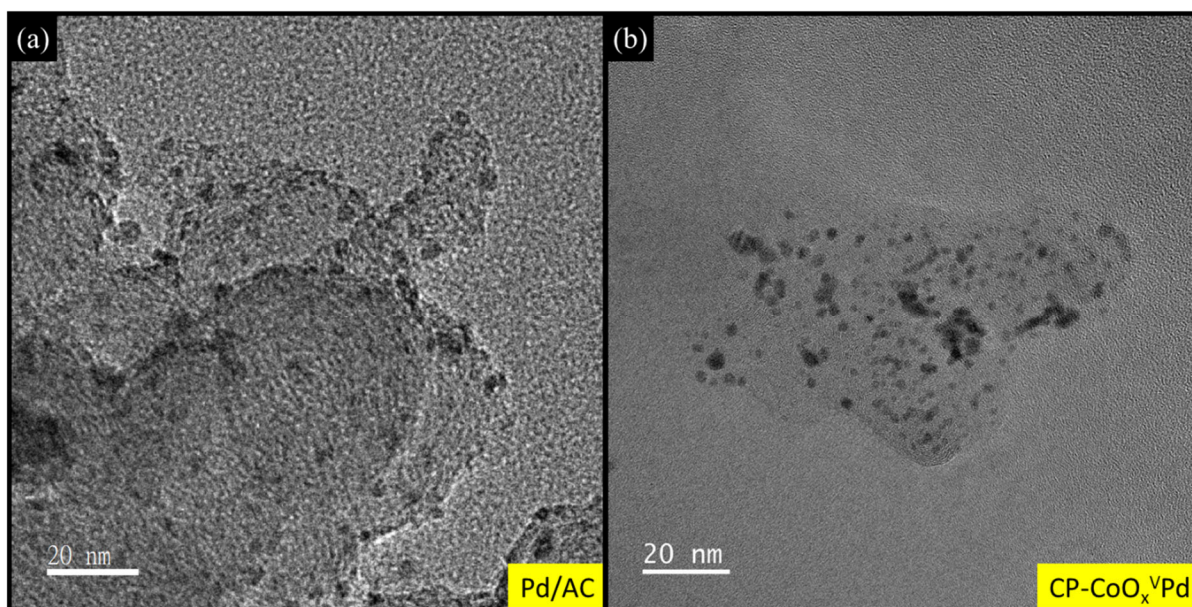

Figure S1. Low magnification TEM image of (a) Pd/AC and (b) CP-CoO$_x$^{V}Pd NCs.

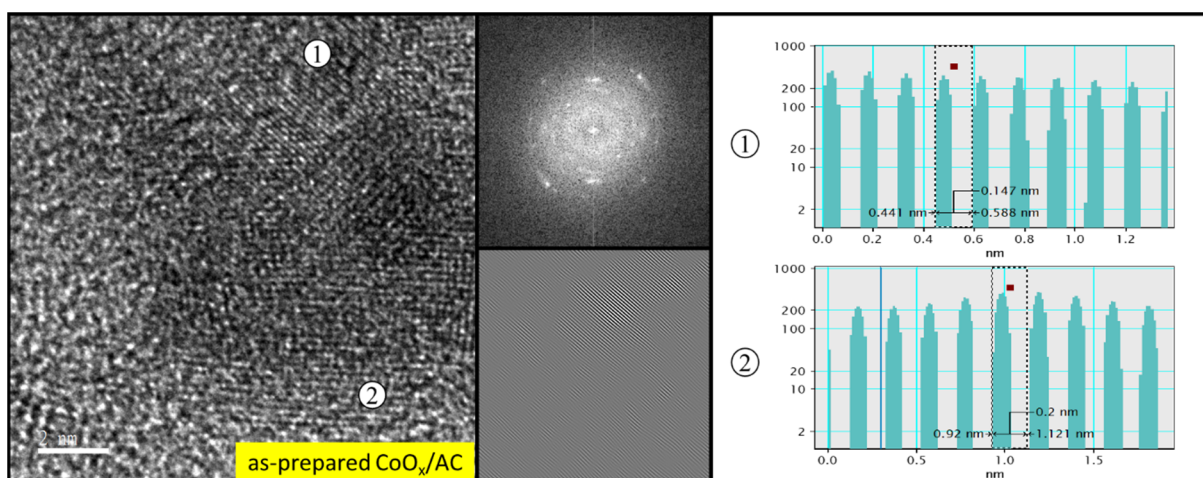## 5. HRTEM image of as-prepared CoO$_x$/AC.

Figure S2. HRTEM images of CoO$_x$/AC. The Forward Fourier Transformed (FFT), Inverse Fourier Transformed (IFT) and the line histogram of are depicted in insets.

6. Model analysis fitting curves compared with experimental FT-EXAFS spectra at Co K-edge.
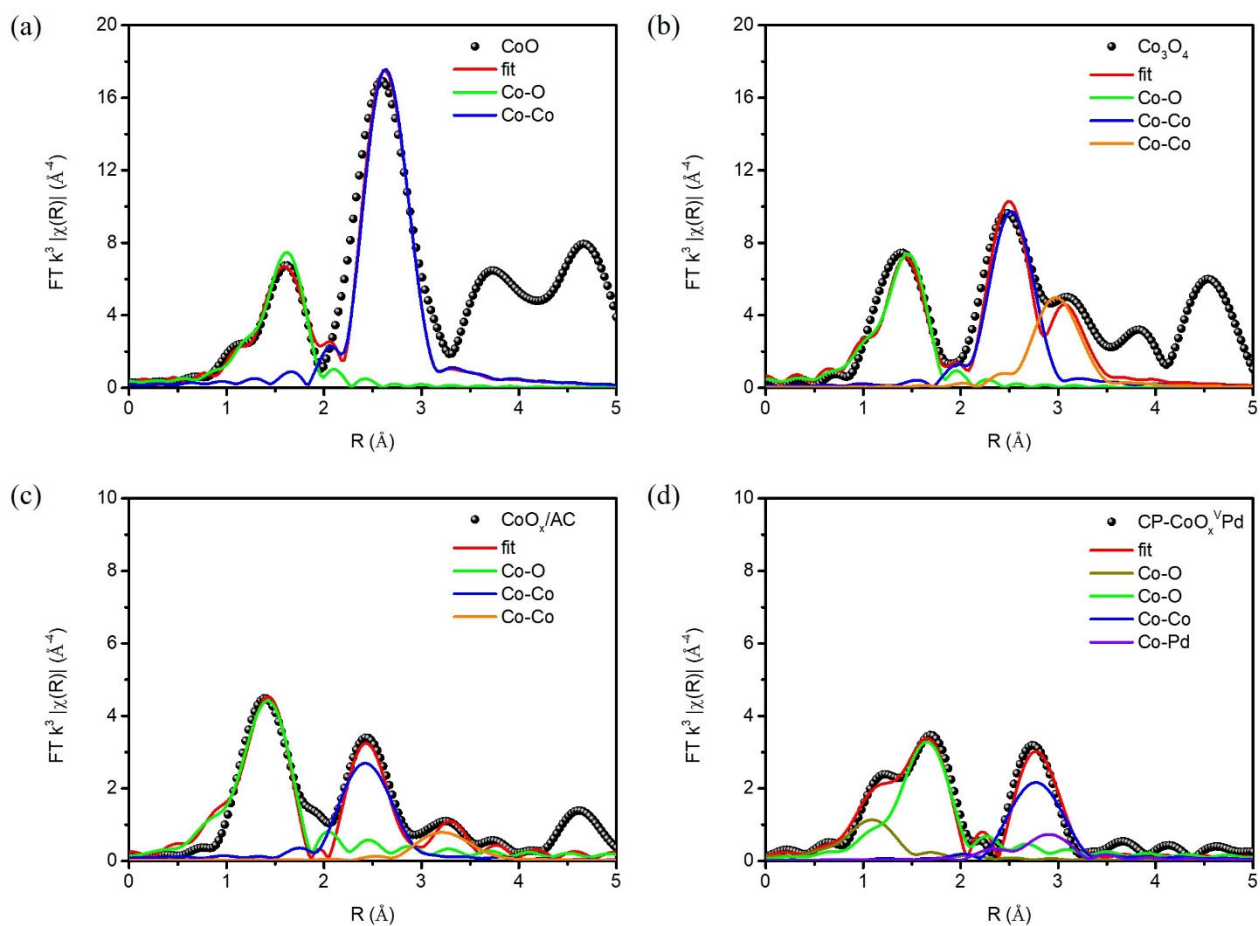

Figure S3. Model analysis fitting curves compared with experimental FT-EXAFS spectra at Co K-edge of (a) CoO, (b) Co_3O_4, (c) CoO_x/AC and (d) CP-CoO_x^VPd NCs.

7. Model analysis fitting curves compared with experimental FT-EXAFS spectra at Pd K-edge.
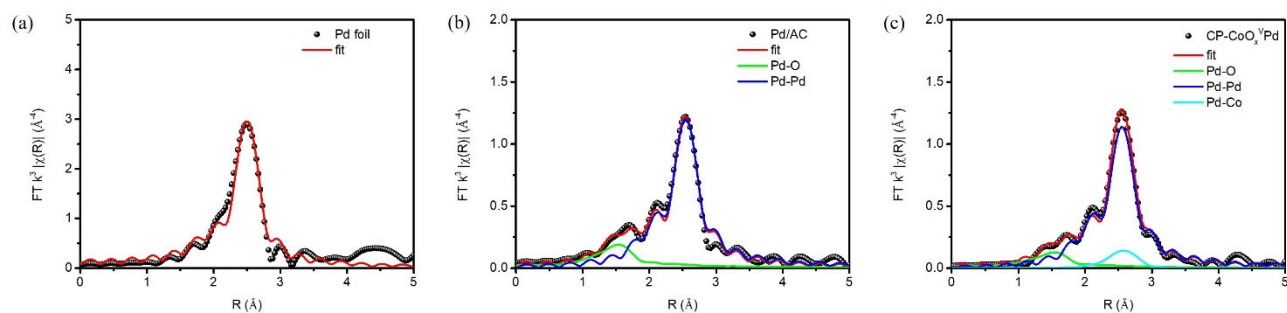

Figure S4. Model analysis fitting curves compared with experimental FT-EXAFS spectra at Pd K-edge of (a) Pd foil, (b) Pd/AC and (c) CP-CoO_x^VPd NCs.

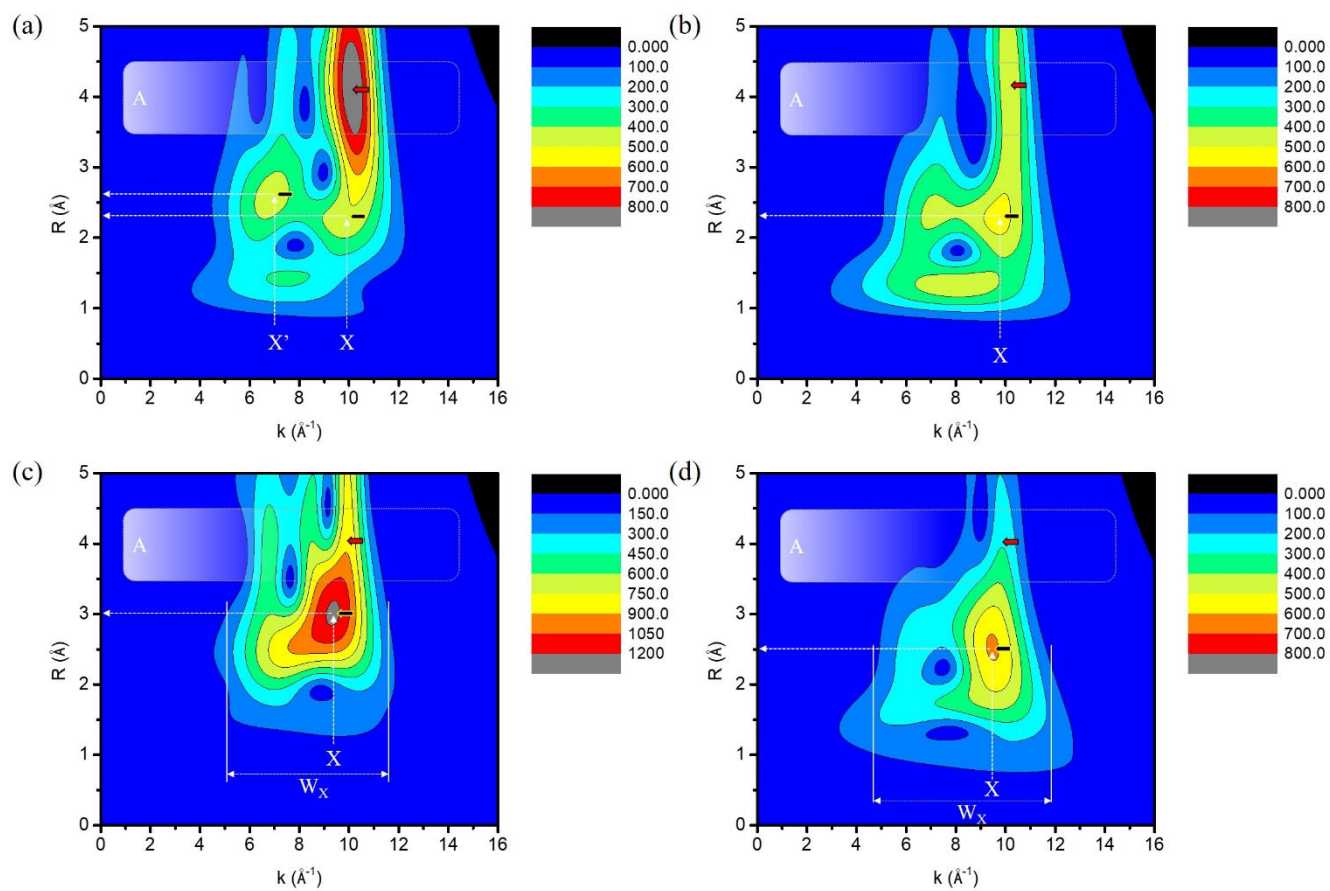## 8. The WT for EXAFS spectrum at Co K-edge

Figure S5. The WT for FT-EXAFS spectrum at Co K-edge. (a) Co_3O_4, (b) CoO_x/AC, (c) CoO and (d) CP-$CoO_x{}^V Pd$ NPs. The intensity of Co_3O_4 and CoO are normalized by 0.4-fold as in FE-EXAFS.

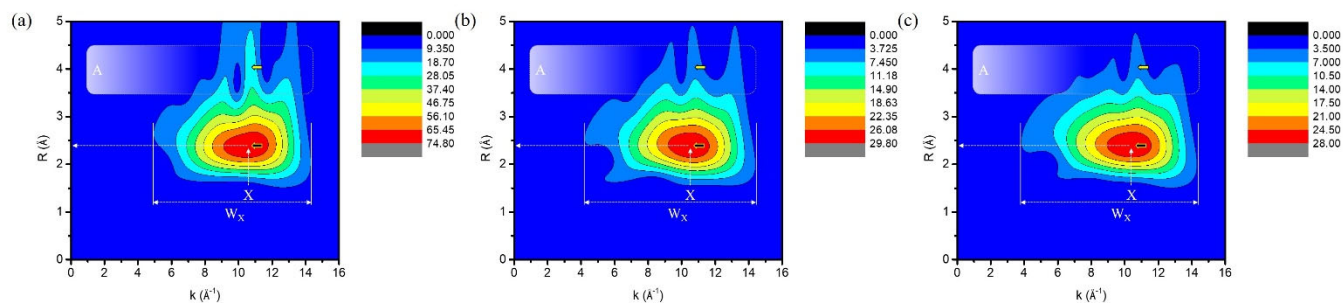## 9. The WT for EXAFS spectrum at Pd K-edge of Pd foil, Pd/AC and CP-CoO$_x$^{V}Pd NCs.

Figure S6. The WT for EXAFS spectrum at Pd K-edge. (a) Pd foil, (b) Pd/AC and (c) CP-CoO$_x$^{V}Pd NCs.

10. X-ray photoelectron spectroscopy of (a) Pd/AC and (b) CP-CoO$_x$^{V}Pd NC NCs at Pd-3d orbital.
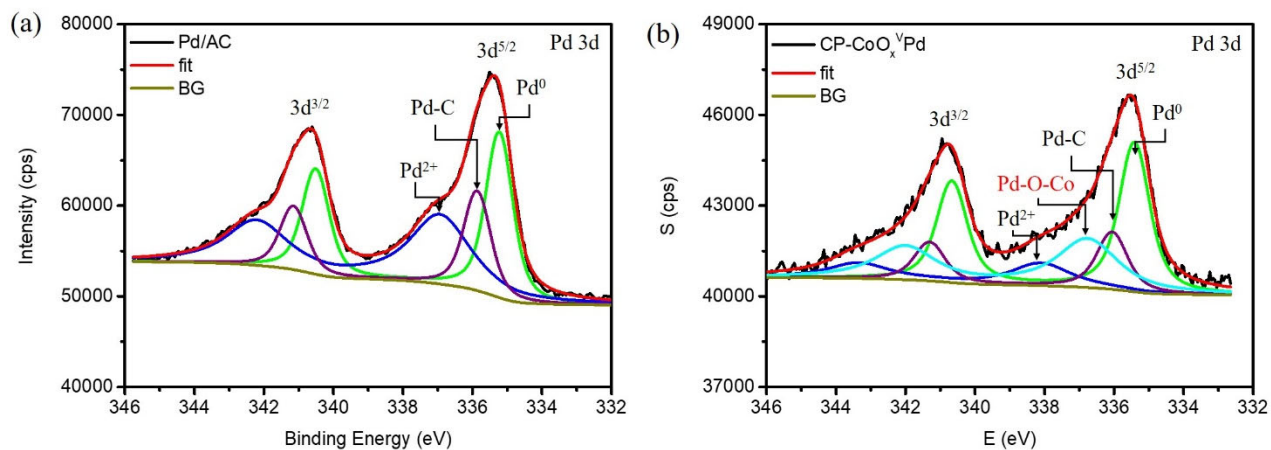

Figure S7. X-ray photoelectron spectroscopy of (a) Pd/AC and (b) CP-CoO$_x$^{V}Pd NCs at Pd-3d orbital.

11. Quantitative results of X-ray photoemission spectroscopy model analysis at Co-2p, O-1s and Pd-3d orbitals of experimental and control NCs.

Table S2. Quantitative results of X-ray photoemission spectroscopy model analysis at Co-2p, O-1s and Pd-3d orbitals of experimental and control NCs.

Catalyst	Elemental chemical states (%)											Ratio	
	Co-O-Pd	Co 2+	Co 3+	C-O	C=O	O^V	O^L	Pd 2+	Pd-O-Co	Pd-C	Pd 0	Co^{2+}/Co^{3+}	O^V/O^L
CoO_x/AC	N/A	52.6	47.4	32.4	42.3	17.2	8.1	N/A				1.11	2.12
CP-$CoO_x{}^VPd$	25.0	31.4	43.6	25.5	36.5	30.7	7.3	13.0	28.5	16.2	42.3	1.29	4.21
Pd/AC	N/A							38.5	N/A	23.1	38.4	N/A	

Catalyst	Binding Energy (eV)										
	Co-O-Pd	Co 2+	Co 3+	C-O	C=O	O^V	O^L	Pd 2+	Pd-O-Co	Pd-C	Pd 0
CoO_x/AC	N/A	782.45	781.17	534.04	532.72	531.84	530.35	N/A			
CP-$CoO_x{}^VPd$	783.58	782.45	781.27	533.88	532.74	531.94	531.17	338.11	336.76	336.05	335.41
Pd/AC	N/A							336.93	N/A	335.23	335.23

12. The gas chromatography (GC) determined CO$_2$RR results for the CP-CoO$_x^V$Pd and control samples (CoO$_x$/AC, Pd/AC and physical mixing of CoO$_x$+Pd).

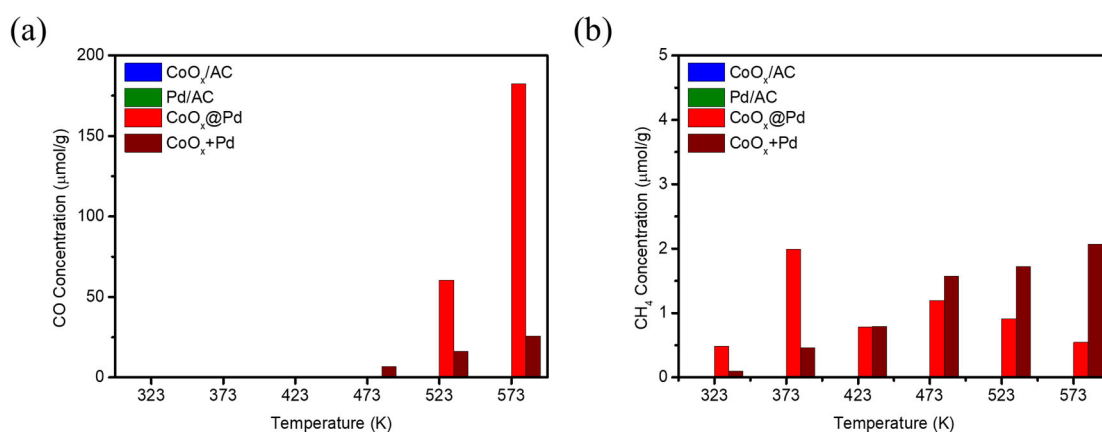**Figure S8**. The gas chromatography (GC) determined CO$_2$RR results for the CP-CoO$_x^V$Pd and control samples (CoO$_x$/AC, Pd/AC and physical mixing of CoO$_x$+Pd). (a) CO and (b) CH$_4$ production yield is measured under 100% CO$_2$ ambient. The GC measurements are conducted under a pressure of near 1 atm from 323 K to 573 K and the concentration is normalized by loading of catalysts (μmol g^{-1}).

13. Calibrated product concentration of CO and CH$_4$ under 100% CO$_2$ and CO$_2$ and H$_2$ mixture ambient from 323 K to 573 K without carrier gas for 12 mg of experimental and reference NCs.

Table S3 Calibrated product concentration of CO and CH$_4$ under 100% CO$_2$ and CO$_2$ and H$_2$ mixture ambient from 323 K to 573 K without carrier gas for 12 mg of experimental sample (CP- CoO$_x$^{V}Pd) and reference samples (CoO$_x$/AC, Pd/AC and physical mixing of CoO$_x$+Pd). The unit of concentration is µmol g^{-1}. The corresponding selectivity of CO (S$_{CO}$) at all temperature is recorded.

Sample	CoO$_x$/AC				Pd/AC				CP- CoO$_x$^{V}Pd				CoO$_x$ + Pd			
	CO$_2$	CO$_2$+3H$_2$			CO$_2$	CO$_2$+3H$_2$			CO$_2$	CO$_2$+3H$_2$			CO$_2$	CO$_2$+3H$_2$		
Temp. (K)	CO	CO	CH$_4$	S$_{CO}$ (%)	CO	CO	CH$_4$	S$_{CO}$ (%)	CO	CO	CH$_4$	S$_{CO}$ (%)	CO	CO	CH$_4$	S$_{CO}$ (%)
323																
373	N/A		N/A		N/A		N/A		N/A	N/A	1.2	0.0	N/A	N/A	0.4	0.0
423										68.2	12.2	84.8			1.8	0.0
473						82.4	1.7	98.0		548.2	25.3	95.6	6.7	4.1	11.8	25.8
523		11.8	0.8	93.7		472.6	9.3	98.1	60.4	1572.9	18.2	98.9	16.3	31.8	18.5	63.2
573		348.2	12.7	96.5		1466.0	27.1	98.2	182.4	3413.5	90.2	97.4	25.8	109.4	9.4	92.1

Reference

1. Ai, X.; Xie, H. M.; Chen, S. M.; Zhang, G. Z.; Xu, B. J.; Zhou, G. L. *International Journal of Hydrogen Energy* 2022, **47**, (33), 14884-14895.
2. Pastor-Pérez, L.; Baibars, F.; Le Sache, E.; Arellano-García, H.; Gu, S.; Reina, T. R. *Journal of CO2 Utilization* 2017, **21**, 423-428.
3. Tarifa, P.; González-Castaño, M.; Cazaña, F.; Monzón, A.; Arellano-García, H. *Fuel* 2022, **319**, 123707.
4. Shen, H. D.; Dong, Y. J.; Yang, S. W.; He, Y.; Wang, Q. M.; Cao, Y. L.; Wang, W. B.; Wang, T. S.; Zhang, Q. Y.; Zhang, H. P. *Nano Research* 2022, **15**, 5831-5841.
5. Zonetti, P. C.; Letichevsky, S.; Gaspar, A. B.; Sousa-Aguiar, E. F.; Appel, L. G. *Applied Catalysis A: General* 2014, **475**, 48-54.
6. Yang, L. Q.; Pastor-Perez, L.; Villora-Pico, J. J.; Sepulveda-Escribano, A.; Tian, F. X.; Zhu, M. H.; Han, Y. F.; Reina, T. R. *Acs Sustainable Chemistry & Engineering* 2021, **9**, (36), 12155-12166.
7. Nityashree, N.; Price, C. A. H.; Pastor-Perez, L.; Manohara, G. V.; Garcia, S.; Maroto-Valer, M. M.; Reina, T. R. *Applied Catalysis B: Environmental* 2020, **261**, 118241.
8. Okemoto, A.; Harada, M. R.; Ishizaka, T.; Hiyoshi, N.; Sato, K. *Applied Catalysis A: General* 2020, **592**, 117415.
9. Price, C. A. H.; Pastor-Perez, L.; Reina, T. R.; Liu, J. *Catalysis Today* 2022, **383**, 358-367.
10. Ronda-Lloret, M.; Yang, L. Q. Q.; Hammerton, M.; Marakatti, V. S.; Tromp, M.; Sofer, Z.; Sepulveda-Escribano, A.; Ramos-Fernandez, E. V.; Delgado, J. J.; Rothenberg, G.; Reina, T. R.; Shiju, N. R. *Acs Sustainable Chemistry & Engineering* 2021, **9**, (14), 4957-4966.
11. Dostagir, N. H. M.; Rattanawan, R.; Gao, M.; Ota, J.; Hasegawa, J. Y.; Asakura, K.; Fukouka, A.; Shrotri, A. *Acs Catalysis* 2021, **11**, (15), 9450-9461.